MAUSAM, **75**, 4 (October 2024), 943-954

MAUSAM

DOI : https://doi.org/10.54302/mausam.v75i4.6348
Homepage: https://mausamjournal.imd.gov.in/index.php/MAUSAM

UDC No. 633:551.573:528.8 (540.51)

Assessment of Spatiotemporal Variations in Actual Evapotranspiration using the pySEBAL Model and Remote Sensing Data in Navsari, Gujarat, India

V. B. VIRANI, NEERAJ KUMAR[*], B. M. MOTE, N. M. CHAUDHARI[**] and J. B. DELVADIYA[***]

Agricultural Meteorological Cell, Navsari Agricultural University, Navsari, Gujarat, India

[*]*Dept. of Agronomy, College of Agriculture, Navsari Agricultural University, Bharuch, Gujarat, India*

[**]*Dept. of Soil Science and Agril. Chemistry, Navsari Agricultural University, Navsari, Gujarat, India*

[***]*Dept. of Agricultural Statistics, Navsari Agricultural University, Navsari, Gujarat, India*

(*Received 11 August 2023, Accepted 17 June 2024*)

e mail: vivekvirani.vv@gmail.com

सार – वाष्पोत्सर्जन (ET), जिसमें पौधों से होने वाला पारसरण और पृथ्वी की सतह से होने वाला वाष्पीकरण दोनों शामिल हैं, जल विज्ञान चक्र का एक महत्वपूर्ण घटक है तथा यह सतह और वायुमंडल के बीच जल और ऊर्जा के आदान-प्रदान को प्रभावित करता है। यह अध्ययन भारत के गुजरात के नवसारी जिले में वास्तविक वाष्पोत्सर्जन (AET) का अनुमान लगाने के लिए भूमि के लिए सतही ऊर्जा संतुलन एल्गोरिथ्म (SEBAL) के अनुप्रयोग की जांच करता है। सतही ऊर्जा संतुलन के सिद्धांतों पर आधारित SEBAL एल्गोरिदम, अव्यक्त ऊष्मा प्रवाह (शुद्ध विकिरण, भू-ऊष्मा प्रवाह और संवेदी ऊष्मा प्रवाह का अवशेष) की गणना करके AET की गणना करता है और इसे मिमी/दिन में परिवर्तित करता है। क्लाउड-मुक्त लैंडसैट 8 उपग्रह चित्रों (30 x 30 मीटर स्थानिक विभेदन) का उपयोग पायथन-निर्मित GRASSGIS सॉफ्टवेयर के वर्चुअल वातावरण में एक्जीक्यूट पीएसईबीएएल मॉडल एल्गोरिदम द्वारा एईटी का अनुमान लगाने के लिए किया गया था। आवश्यक डेटा में पवन गति (मी./से.), संदर्भ वाष्पोत्सर्जन (RET), उपग्रह ओवरपास के दौरान तात्कालिक RET दर (मि.मी./घंटा) तथा डिजिटल उन्नयन मॉडल (DEM) डेटा शामिल हैं। परिणामों से पता चला कि AET का संबंध शुद्ध सौर विकिरण, भूमि सतह तापमान, एल्बिडो, भू और संवेदी ताप प्रवाह जैसे कारकों से है। AET दरों में महत्वपूर्ण स्थानिक-कालिक विविधताएं देखी गई, उच्चतम AET दरें मई माह में देखी गईं, तथा शुद्ध विकिरण की मात्रा कम होने के कारण AET दरों में कमी देखी गई। अध्ययन क्षेत्र में, प्रमुख AET दर गर्मियों के महीनों के दौरान 4 से 6 मिमी/दिन और सर्दियों के महीनों के दौरान 2 से 3 मिमी/दिन तक होती है। यह पैटर्न कुल अध्ययन क्षेत्र के 65% से अधिक क्षेत्र को कवर करता है। मई में, अध्ययन क्षेत्र के लगभग 15-20% हिस्से में AET दरें PET दरों के साथ काफी हद तक संरेखित थीं, जो संभवतः आसन्न जल कमी की चिंताओं का संकेत है। निष्कर्ष में, pySEBAL एल्गोरिथ्म ने विस्तृत और विषम क्षेत्रों में AET का अनुमान लगाने की अपनी क्षमता का प्रदर्शन किया और विशेष रूप से वहां प्रभावी रहा जहां लाइसीमीटर और एडी कोवैरिएंस उपकरण उपलब्ध नहीं हैं।

ABSTRACT. Evapotranspiration (ET), encompassing both transpiration from plants and evaporation from the Earth's surface, is a vital component of the hydrological cycle and influences water and energy exchanges between the surface and the atmosphere. This study investigates the application of the Surface Energy Balance Algorithm for Land (SEBAL) to estimate actual evapotranspiration (AET) over the Navsari district of Gujarat, India. The SEBAL algorithm, based on the principles of surface energy balance, calculates AET by calculating latent heat flux (residual of net radiation, ground heat flux and sensible heat flux) and its convert into mm/day. Cloud-free LANDSAT 8 satellite images were utilized (30 x 30 m spatial resolution) to estimate AET by execute pySEBAL model algorithms within virtual environment of Python-built GRASSGIS software. The required data includes windspeed (m/s), reference evapotranspiration (RET), instantaneous RET rate (mm/hr) during satellite overpasses and digital elevation model (DEM) data. The results showed that AET correlated with factors such as net solar radiation, land surface temperature, albedo, ground and sensible heat flux. The AET rates exhibited significant spatiotemporal variations, highest AET rates were observed during the month of May and there was a decrease in AET rates as the amount of net radiation reduced. Across the study area, the dominant AET rate ranges from 4 to 6 mm/day during the summer months and from 2 to 3 mm/day during the winter months. This pattern encompasses more than 65% of the total study area. In May, approximately 15-

20% of the study area exhibited AET rates closely aligning with PET rates, possibly signaling impending water scarcity concerns. In conclusion, the pySEBAL algorithm demonstrated its potential for estimating AET over large and heterogeneous regions and especially effective where lysimeter and Eddy Covariance instruments are not available.

Key words – SEBAL, Actual evapotranspiration, Spatiotemporal dynamics, Energy balance, Remote sensing and GRASSGIS.

1. Introduction

Evapotranspiration is indeed the biophysical process that involves water losses occurring from both plants or living surface (transpiration) and the earth surface (evaporation). It is a crucial component of the hydrological cycle and plays a significant role in the water and energy transfer (in form of latent heat) between the earth surface and the atmosphere. In the hydrological cycle, by the evapotranspiration (ET) process, water transforms into water vapor form by absorbing heat from surrounding. This stored heat is released during process of condensation and precipitation and that influencing the weather patterns and regional climates. This continuous of hydrological cycle plays an important role in maintaining health of ecosystems, distributing water resources globally and restoring the world's freshwater resources. Three conditions must be required for ET to occur: there must be enough soil moisture, a sufficient vapour pressure gradient and enough energy to trigger the phase shift. If any of these conditions are not met, ET will not occur (Bhatt and Khera, 2006).

The computation of evapotranspiration holds significant importance across diverse fields such as hydrology, agriculture, energy budget analysis and climate research (Ajjur and Al-Ghamdi, 2021). Accurate estimation of evapotranspiration is vital in various applications, such as determining irrigation needs and runoff volumes (Li *et al*., 2020), analysing the energy budget of the earth-atmosphere system (Diak *et al*., 2004), improving atmospheric circulation model predictions (Pielke *et al.*, 1998) and characterizing climate patterns (Wang *et al*., 2017). Furthermore, accurate estimations of evapotranspiration empower farmers to apply optimal crop water requirements, resulting in water and energy conservation. On the contrary, inaccurate estimations can lead to improper irrigation practices, such as water shortages or water logging, negatively impacting crop yields (Rahimi- Moghaddam *et al*., 2018).

Estimating evapotranspiration (ET) over large and heterogeneous areas poses a significant challenge because ground measurement networks, such as lysimeter and Eddy Covariance method, have limited spatial coverage (McShane *et al*., 2017) and are expensive. Over the past two decades, several remote sensing-based energy balance models, including SEBAL (surface energy balance algorithm for land) (Bastiaanssen *et al*., 1998), TSEB (Two-Source Energy Balance) (Norman *et al.*, 1995), METRIC (Mapping Evapotranspiration at high Resolution with Internalized Calibration) (Allen *et al*., 2007), SSEBop (Simplified Surface Energy Balance operational) (Senay *et al*., 2013) and SEBS (Surface Energy Balance System) (Su, 2002), have emerged as reliable and consistent alternatives for estimating evapotranspiration over diverse temporal and large spatial scales. Evapotranspiration (ET) is determined using an energy balance approach at the surface, which accounts for the energy consumed by the ET process, known as latent heat (LE). This is achieved by subtracting the ground heat flux (G) and sensible heat flux (H) from the net radiation (Rn) (Zhang *et al.*, 2011). SEBAL, among various models, has demonstrated successful applications worldwide across diverse climates and land cover conditions, particularly in water resources management, providing reliable and consistent results (Wagle *et al*., 2017).

This study utilized cloud-free satellite images from LANDSAT 8 with a spatial resolution of 30 x 30 m. Geo processing of the LANDSAT 8 images to compute Actual Evapotranspiration (AET) was performed by running the SEBAL (Surface Energy Balance Algorithm for Land) model in Python built GRASSGIS software.

2. Study area and data

2.1. *Study area*

In the present study, Navsari district of Gujarat was selected which situated between 20°32' to 21°05' North Latitude and 72°42' to 73°30' East Longitude (Fig. 1). The area is situated in the west part of India and fall under South Gujarat heavy rainfall agro climatic zone. The total geographical area of Navsari district is 2204 km^2. Over the last three decades, the region under study, where the IMD weather station is located at Navsari Agricultural University, experienced an average annual rainfall of approximately 1731 mm. Additionally; the average maximum temperature in the area was about 32.11 ℃, while the average minimum temperature was 25.5 ℃.

2.2. *Details of data*

The current research utilized a combination of space-borne data obtained from LANDSAT 8 satellites, station-based meteorological data and reference evapotranspiration (RET) data. These three data sources were utilized to obtain the actual evapotranspiration (AET) results using the SEBAL model for the study area.

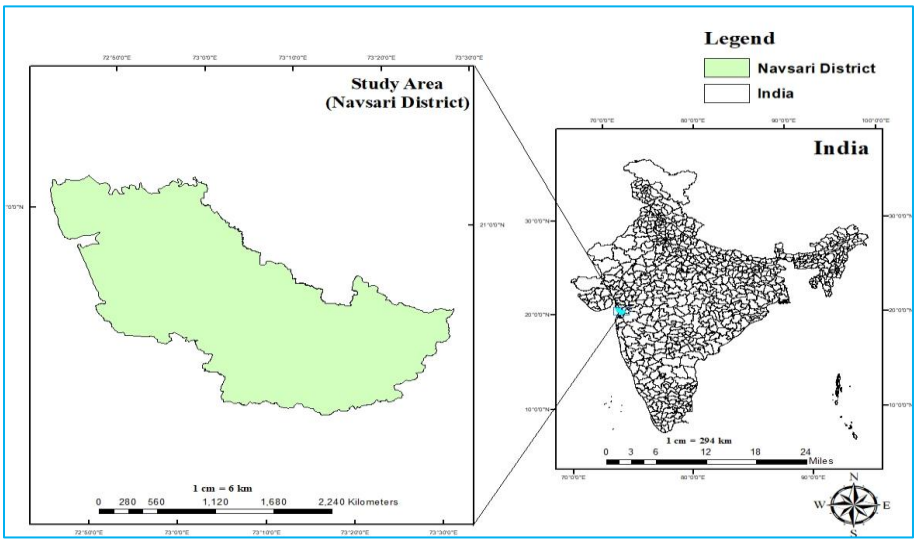

Fig. 1. Location map of study area.

The digital elevation model (DEM) data was obtained by downloading it from the https://earthexplorer.usgs.gov/ website (select study area > Data set > Digital elevation > SRTM), which is representation of the bare ground topography of the earth, which does not include trees, buildings, or any other surface objects. The meteorological data, including maximum and minimum temperature (°C), wind speed (m/s), relative humidity (%) and sunshine hours (BSSH), were utilized to calculate the instantaneous reference evapotranspiration (RET rate in mm/hr.) at the time when the satellite passed over the study area. Additionally, the reference evapotranspiration (in mm/day) on the date of the satellite passing over the study area was also required. Landsat 8 datasets (30 m resolution) of eleven bands (satellite path 148 and row 46) were downloaded from https://earthexplorer.usgs.gov/for the study (in this study LANDSAT collection 2 level 1 data was used). The months were selected based on the availability of cloud-free Landsat 8 images to ensure accurate data for the study period.

3. Methodology adopted

3.1. *SEBAL algorithm description*

SEBAL algorithms estimates AET using remote sensing datasets by deriving latent heat (LE) as a residual of the surface energy balance equation (Equation 1). The SEBAL algorithms are primarily derived from the following references: Bastiaanssen *et al.*, 1998; Bastiaanssen, 2000; Waters, 2002; Sun *et al.*, 2011; Allen *et al.*, 2013; Silva *et al.*, 2016; Beg *et al.*, 2016 and Caiserman *et al.*, 2021.

$$LE = Rn - H - G \quad (1)$$

where, Rn is the net radiation (Equation 2), H is the sensible heat flux (Equation 11) and G is the soil heat flux (Equation 9). The step-by-step procedure to estimating surface energy balance components are given below.

Net radiation (Rn): Net radiation is computed by subtracting the portion of outgoing and incoming longwave radiation from the incoming shortwave radiation.

$$Rn = Rs\downarrow (1 - \alpha) + R_L\downarrow - R_L\uparrow - (1 - \varepsilon_s) R_L\downarrow \quad (2)$$

where, RS↓ matches to the incoming shortwave radiation in Wm^{-2} (Equation 3), $R_L\uparrow$ is outgoing long wave radiation (Wm^{-2}) (Equation 4), $R_L\downarrow$ is incoming long wave radiation (Wm^{-2}) (Equation 6), α is a surface albedo (Equation 8) and ε_s is a surface emissivity (Equation 5).

$$Rs\downarrow = Gsc * \cos\theta * dr * \tau_{sw} \quad (3)$$

where, G_{Sc} is solar constant (1367 Wm^{-2}), θ is the solar incidence angle ($\theta = 90 - \phi$), ϕ is solar elevation angle (value given in metadata file), dr is Inverse earth-sun distance (value given metadata file) and τ_{sw} is atmospheric transmissivity, (formula for calculating $\tau_{sw} = 0.75 + 2 \times 10^{-5} \times$ elevation of station (m)).

$$R_L\uparrow = \varepsilon_s * \sigma * LST^4 \quad (4)$$

where, ε_s is surface emissivity (dimensionless), σ is the Stefan-Boltzmann constant (5.67×10^{-8} $Wm^{-2}K^{-4}$) and LST is land surface temperature (K).

$$\varepsilon_s = 1.009 + 0.047 * \ln (NDVI) \quad (5)$$

NDVI > 0, otherwise, emissivity is assumed to be zero (*e.g.*, water).

$$R_L\downarrow = \varepsilon_a * \sigma * T_a \quad (6)$$

where, ε_a is atmospheric emissivity (= 0.85 $(-\ln\tau_{sw})^{0.09}$) and T_a is near surface air temperature (K).

surface albedo (α): First calculate spectral radiance (Lλ) and spectral reflectance (ρ_λ) at TOA for each band (from 2 to 7 for LANDSAT 8) of satellite and then calculate the albedo at TOA (α_{TOA}) (Equation 7).

$$\alpha_{TOA} = \sum (\omega_\lambda * \rho_\lambda) \quad (7)$$

where, ω_λ = constant value of weighting coefficient of each band (from 2 to 7).

The computation of the surface albedo (α) by following Equation 8.

$$\alpha = \alpha_{TOA} - \alpha_{path\_radiance} / \tau_{sw}^2 \quad (8)$$

where, $\alpha_{path\_radiance}$ is the average portion of the incoming solar radiation across all bands that is back-scattered to the satellite before it reaches the earth's surface (values for $\alpha_{path\_radiance}$ range between 0.025 and 0.04).

Ground heat flux (G): It is a rate of heat storage into the soil due to conduction. It is calculated as function of net radiation, surface albedo and vegetation cover.

$$G = [LST + 273/\alpha] * [(0.0038\alpha + 0.0074\alpha^2) * (1 - 0.98NDVI^4) * Rn] \quad (9)$$

where, LST is a land surface temperature (K) (Equation 10), NDVI stands for Normalized Difference Vegetation Index.

$$LST = BT / [1 + W * (BT / 14380) * \ln(\varepsilon_s)] \quad (10)$$

where, BT is brightness temperature at TOA (K) and W = Wavelength of emitted radiance (value of LANDSAT8 Band 10 is 10.89 μm).

Sensible heat flux (H): It is referring to the transfer of heat energy between the earth surface and the atmosphere through convection and conduction due to temperature difference. The sensible heat flux is difficult to calculate because of values of r_{ah} and dT are unknowns (Equation 11). The calculation of sensible heat flux (H) by the following of an iterative process due to the interdependence between the aerodynamic resistance (r_{ah}) and sensible heat flux (Sawadogo *et al.*, 2020). Initially, the iteration assumes a neutral atmospheric condition, providing a first estimation of sensible heat flux (H) under neutral condition and this value use for calculation of Monin Obukhov length (Fig. 2). SEBAL model uses Monin- Obukhov theory in its iteration process to address atmospheric instability or stability impact on aerodynamic resistance (r_{ah}). The iteration corrects r_{ah} value by incorporating stability corrections for momentum and heat transport based on atmospheric conditions (Waters, 2002), yielding new sensible heat flux (H) values. SEBAL performs multiple iterations until the value for aerodynamic resistance (r_{ah}) stabilizes (Sawadogo *et al.*, 2020). Flow chart of the iterative process for the calculation of sensible heat (H) is depicted in Fig. 2.

$$H = \rho_{air} * Cp * dT / r_{ah} \quad (11)$$

where ρ_{air} is the air density (kg m^{-3}), Cp is the specific heat of air at constant pressure (=1004 J kg^{-1} K^{-1}), dT is the vertical near surface temperature difference (K), r_{ah} is the aerodynamic resistance to heat transport (s m^{-1}) between two height (z_1 and z_2) and a and b are empirical coefficients (Fig. 2).

The SEBAL model calculates dT for each pixel using a linear relationship (dT = a + b * LST), where coefficients a and b are determined by selecting two extreme temperature pixels, namely hot and cold pixels (Water, 2002). The cold pixel represents a well-irrigated crop area with low land surface temperature, high NDVI and low surface albedo, assuming all available energy is used to evaporate water (LE = Rn - G) and H = 0 (dT value at cold pixel will be around zero except semi-arid and arid area). Currently, the suggested approach involves choosing a cold pixel situated in a well-watered agricultural field with good crop growth (Mkhwanazi *et al*., 2015).

An ideal candidate for the hot pixel would be a pixel with a significantly high temperature, indicating extreme dryness where the available energy at the surface is utilized to heat both the surface and the air above, due to the absence of available water for evaporation (high surface albedo) (Mkhwanazi *et al*., 2015). Additionally, the chosen pixel should represent a bare surface with minimal biomass, evident by a very low NDVI value. A dry agricultural area or bare soil is recommended and care should be taken that do not selected highway and building area. Hot pixel is assumed to have LE of zero, and a large dT value (Bastiaanssen *et al*., 1998). These reference pixels anchor the calculations for all other pixels within the defined extreme conditions range. The method outlined by Saboori *et al.*, 2021 involves the process of selecting hot and cold reference pixels. Fig. 3 showcases the chosen reference hot and cold pixel.

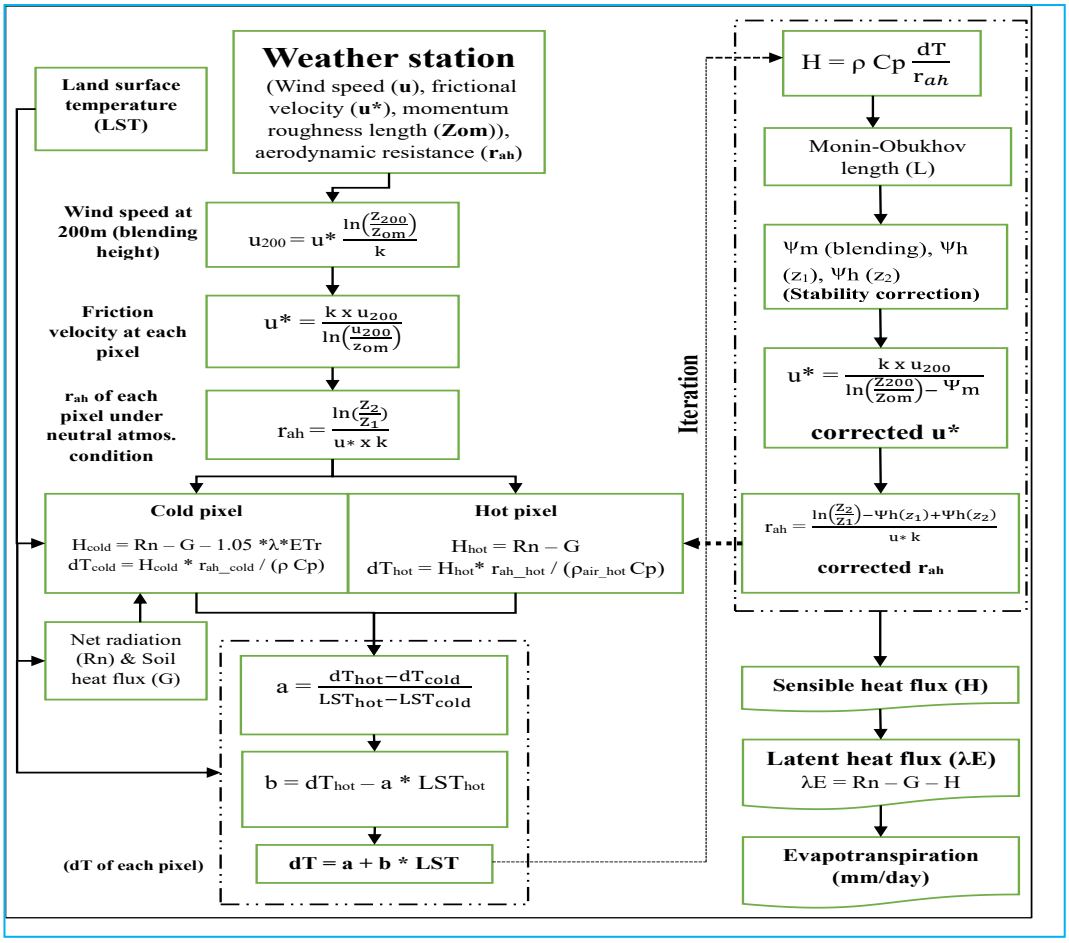

Fig. 2. Flow chart of the iterative process for the calculation of sensible heat (H) (Water, 2002).

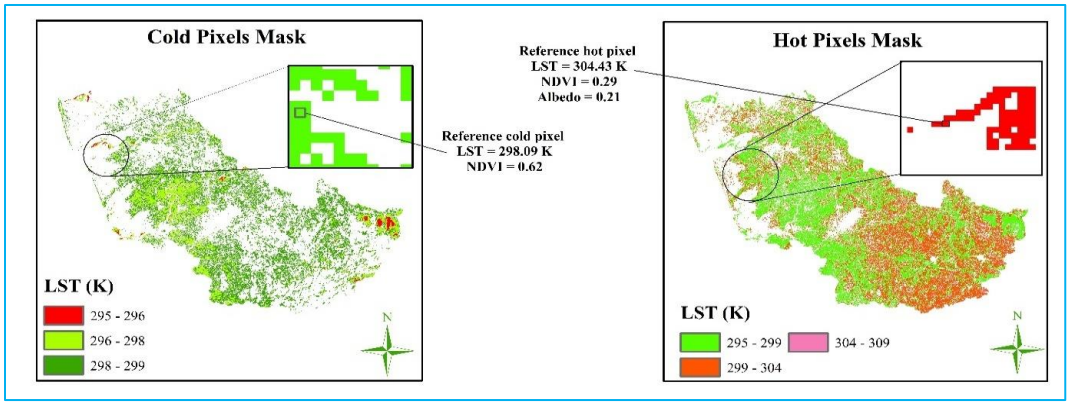

Fig. 3. Selected the reference cold and hot pixel for sensible heat flux (H) calculation.

Evapotranspiration estimation: Using the instantaneous net radiation (Rn), sensible heat flux (H) and ground heat flux (G) at the satellite overpass time, the instantaneous evaporative fraction (EFi) can be computed following Equation 12. Subsequently, the instantaneous evaporative fraction (EF_i) can be converted into the daily evaporative fraction (EF_{24}) using Equation 13, wherein an advective factor Ω is utilized to minimize errors arising from increased ETa during the afternoon (Xue *et al.*, 2020)

$$EF_i = \frac{Rn - H - G}{Rn - G} \quad (12)$$

$$EF_{24} = \Omega \times EF_i \quad (13)$$

where, Ω is calculated as:

$$\Omega = 1 + 0.985 \text{ x EFi x } \{\exp [0.08 \text{ x } (e_s - e_a)] -1\}$$

where, e_s refers to the saturated vapor pressure at the air temperature above the canopy reference height, e_a represents the actual vapor pressure above the canopy height. Using this data, SEBAL computes the daily ETa for each pixel:

$$ET_{24} = \frac{8.64 \text{ x } 10^7 \text{ x } \Omega \text{ x } EF_i \text{ x } (Rn_{24} - G_{24})}{\lambda \text{ x } \rho_w} \quad (14)$$

where, ET_{24} is daily ET on date of satellite pass (mm/day), ρ_w is density of water (kg/m^3), λ is latent heat of vaporization (J/kg), Rn_{24} is daily average net radiation (W/m^2) (Equation 15) and G is a daily average ground heat flux (W/m^2).

$$Rn_{24} = [(1-\alpha) \text{ x } R_a - 110] \text{ x } \tau_{sw} \quad (15)$$

where, Ra is daily extra terrestrial solar radiation (W/m^2)

3.2. *Use of python and GRSSGIS to run SEBAL algorithms*

To simplify the frequent calculations of SEBAL, we use Python script (v3.9.5) (Fig. 4) and it was run by using the GRSSGIS 8.2 software. The output of SEBAL model will be stored in GRASSGIS software. Fig. 4 illustrates the step-by-step guide for configuring the Python environment, locating the Python script source, setting up the necessary paths and specifying input data within the GRASSGIS software. It demonstrates the procedure to run the Python script seamlessly in the GRASSGIS environment, facilitating the efficient execution of SEBAL calculations.

4. Result and discussion

4.1. *Evaluation of SEBAL-derived outcomes*

As per Table 1, seven satellite images from the LANDSAT 8 were used for the study and these images were acquired during the timeframe spanning from October 2022 to May 2023. The SEBAL outcomes for the date of January 15, 2023, are visually represented in the accompanying Fig. 5, while a numerical summary for all processing dates is presented in the provided Table 1. The results indicate that the net solar radiation, land surface temperature, albedo, ground and sensible heat flux are positively correlated with the rate of AET, while latent heat flux, crop coefficient and NDVI are negatively correlated with the rate of AET (Table 1). Intriguingly, regions depicted in Fig. 5 with elevated actual evapotranspiration (AET) rates exhibit comparatively low or negative sensible heat flux, accompanied by high latent heat flux, high NDVI and crop coefficients and relatively low land surface temperatures. The observed relationship between AET and the pySEBAL-derived products is consistent with expectations. While Table 1 presents average values for each raster pixel, Fig. 5 allows for a more detailed visualization of the relationships between these parameters, revealing patterns that might not be apparent from the average raster values alone. Areas with high land surface temperatures typically exhibit low NDVI values, indicating sparse or absent vegetation cover. This lack of vegetation cover significantly impacts energy partitioning, leading to increased sensible heat flux and decreased latent heat flux. The absence of vegetation cover prevents the conversion of net radiation into latent heat flux through evapotranspiration. Consequently, the energy from net radiation is primarily partitioned into ground heat flux and sensible heat flux, contributing to the elevated land surface temperatures (Fig. 5). Areas with high NDVI values exhibit a significant water presence and partitioning of net radiation where a significant portion is converted into latent heat flux, with some portion also going towards ground heat flux. This efficient partitioning of energy into latent heat flux results in a high AET rate and contributes to maintaining relatively moderate land surface temperatures (Fig. 5). In months such as October, November and January, even when NDVI is high, the AET rate comparatively remains low. This discrepancy could be attributed to reduced incoming solar radiation during these months, impacting the overall evapotranspiration process (Table 1). A study by Bansouleh *et al.* (2015) revealed a discrepancy in actual evapotranspiration (AET) rates between irrigated maize plots (high NDVI) and mountainous regions through SEBAL model. The researchers observed a significantly higher AET rate in the irrigated maize fields compared to the low-NDVI mountainous areas.

4.2. *Spatial and temporal variation of AET*

The tracking of actual daily evapotranspiration is importance to study, how water and energy interact on the surface (Seller *et al.*, 1996). Understanding how evapotranspiration changes over time and in different places is crucial for managing limited water resources effectively. Therefore, in this study, once we calculated the Actual Evapotranspiration (AET) using the SEBAL method, we generated maps to visually represent its changes over time (month to month) in Fig. 6 and numerically represent across study area in Table 2. Table 2 highlights how different AET ranges are distributed across specific areas on each date. This spatial variation showed diversity in water use, vegetation health and climate conditions across the studied area. The highest rate of actual evapotranspiration (AET) occurred in the month of May. During this period, an area of 312.40 km^2

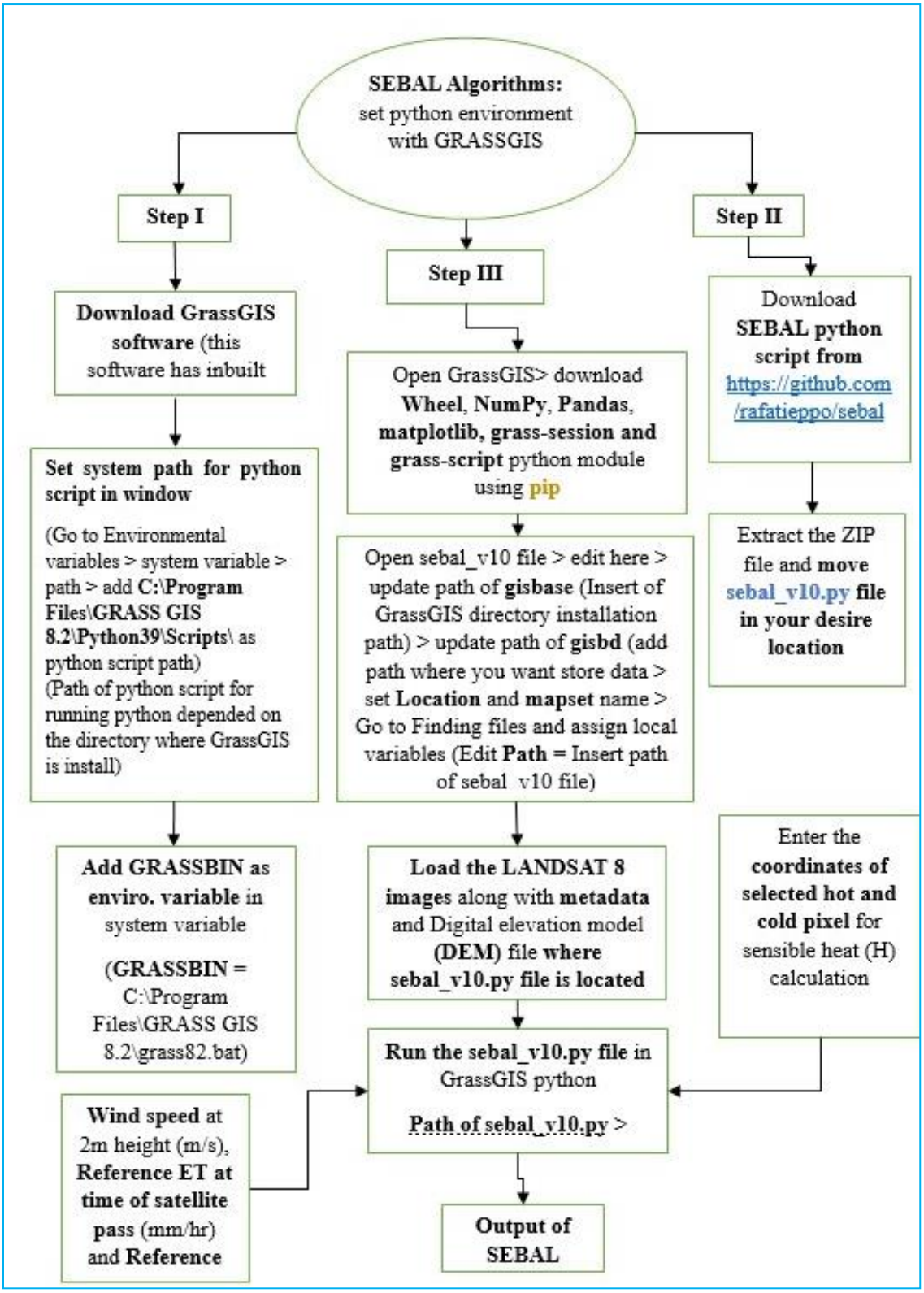

Fig. 4. Flow chart of procedure to setting up python environment with GRASS GIS software.

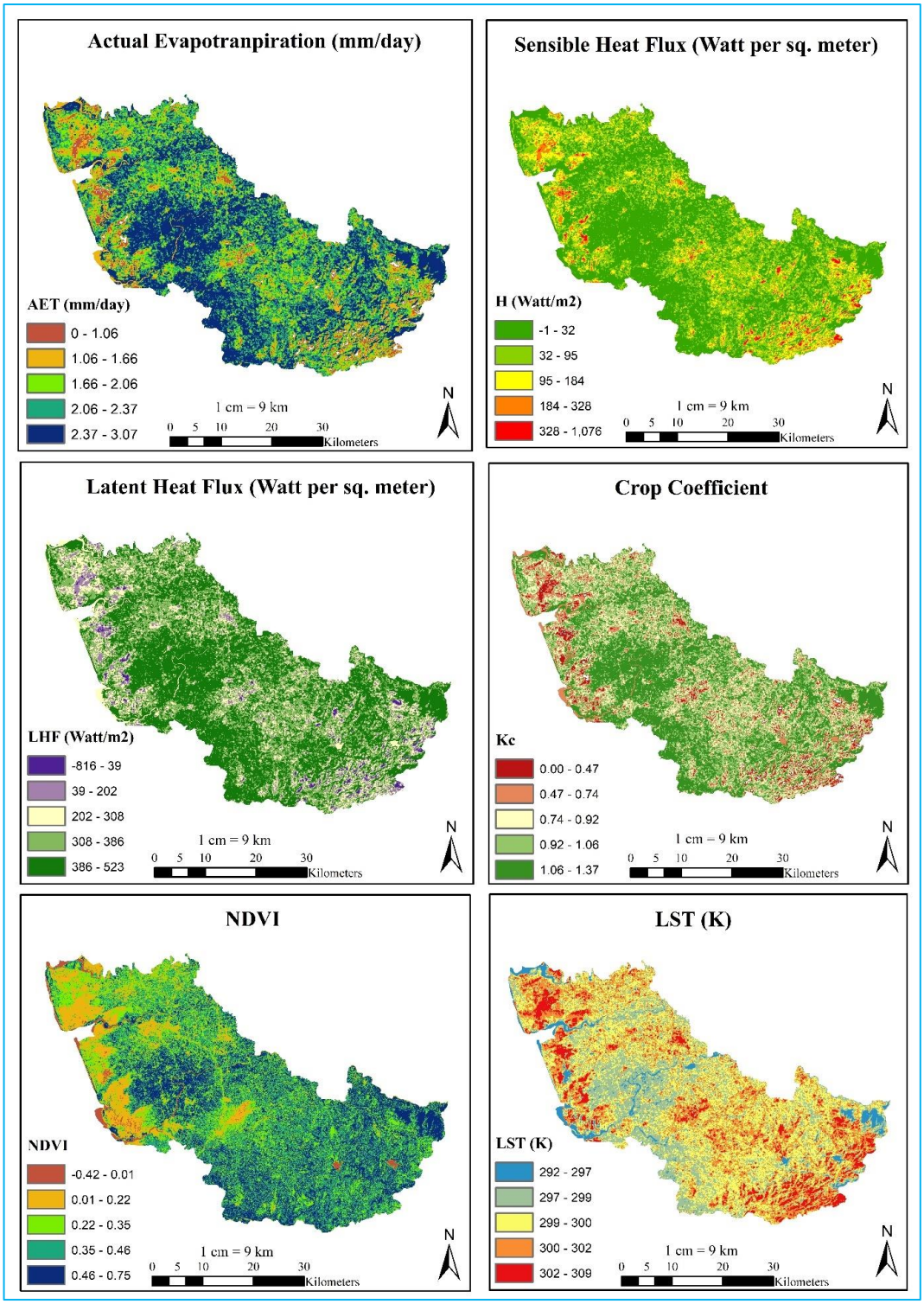

Fig. 5. Visual outcomes of SEBAL illustrating the AET rate, surface energy fluxes, crop coefficient, NDVI and land surface temperature distribution on January 15, 2023.

.

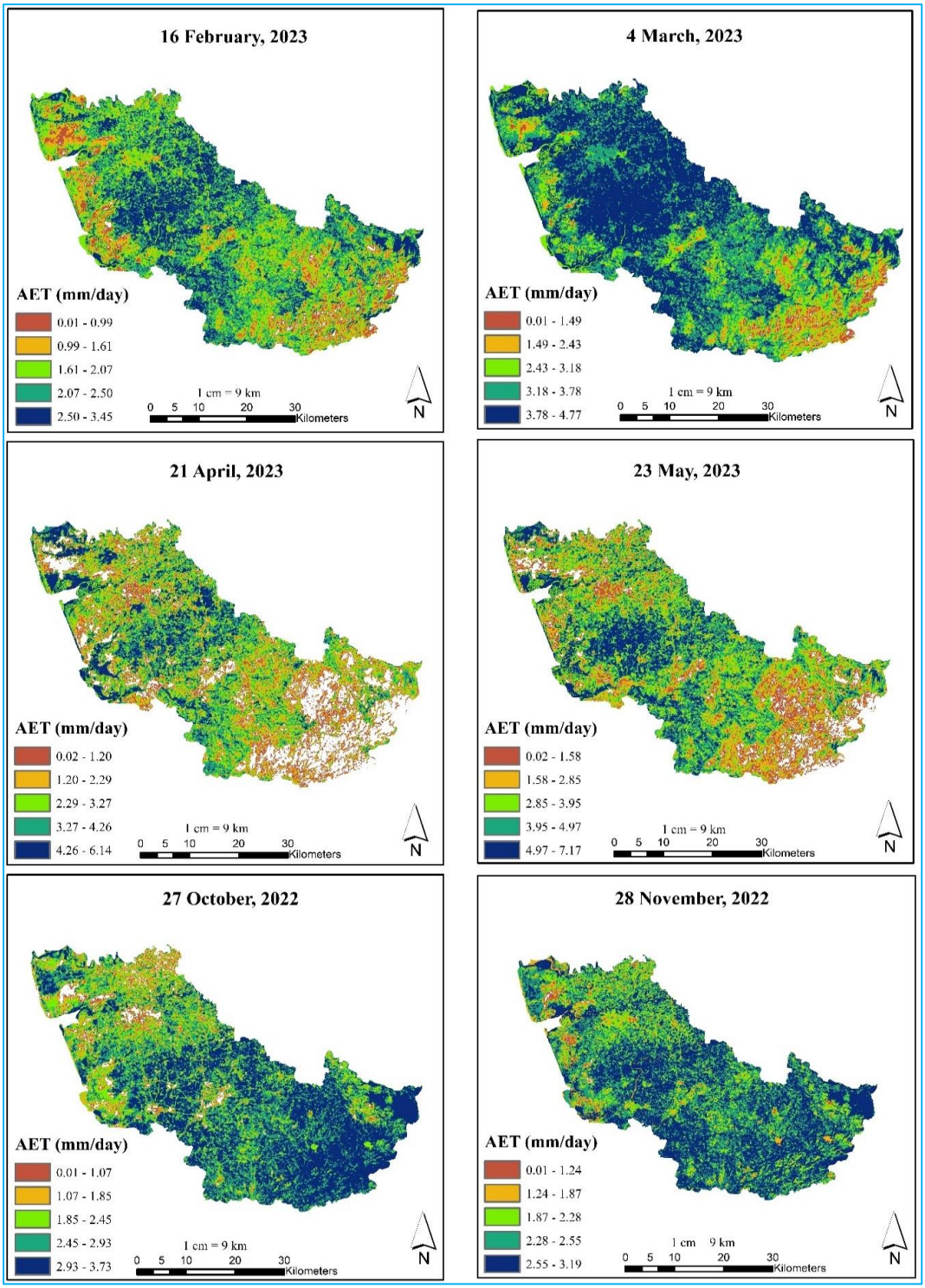

*****White areas indicate absence of actual evapotranspiration

Fig. 6. Spatiotemporal variations in actual evapo-transpiration (mm/day) across study area.

TABLE 1

Outcomes obtained via SEBAL with pixel representation are summarized as average values for Navsari district

Sensing date	ET_{24} (mm/day)	NDVI	Surface albedo (%)	LST (K)	Rn (W/m^2)	H (W/m^2)	G (W/m^2)	LE (W/m^2)	Crop coefficient
27/10/2022	2.53	0.51	0.16	303.07	560.79	94.14	80.11	386.51	0.70
28/11/2022	2.40	0.43	0.15	303.00	502.98	24.85	74.12	404	0.77
15/01/2023	2.08	0.37	0.16	300.03	477.70	57.41	65.83	354.71	0.93
16/02/2023	2.02	0.35	0.15	309.22	514.07	97.00	93.07	323.97	0.61
04/03/2023	3.46	0.23	0.22	306.16	525.10	49.47	97.41	378.20	0.89
21/04/2023	2.90	0.36	0.18	310.69	755.61	271.13	117.13	220.20	0.44
23/05/2023	3.27	0.36	0.20	309.50	602.59	194.21	114.73	293.62	0.63
Correlation (r)		-0.49	0.93	0.43	0.42	0.34	0.67	-0.21	-0.08

TABLE 2

Diverse spatial patterns of daily actual evapotranspiration (ETa) in the study area

Date	ETa	No ETa	0-1	1-2	2-3	3-4	4-5	5-6	6-7
15/01/2023	Area (km^2)	15.77	80.11	614.06	1493.00	0	0	0	0
	Area (%)	0.71	3.96	27.87	67.77	0	0	0	0
16/02/2023	Area (km^2)	19.27	136.59	775.01	1236.05	35.82	0	0	0
	Area (%)	0.87	6.20	35.18	56.10	6.16	0	0	0
04/03/2023	Area (km^2)	5.54	31.47	97.80	332.09	1157.53	578.54	0	0
	Area (%)	0.25	1.42	4.43	15.07	52.54	26.26	0	0
21/04/2023	Area (km^2)	348.91	250.06	337.98	420.53	467.87	303.96	73.49	0
	Area (%)	15.83	11.34	15.34	19.08	21.23	13.79	3.32	0
23/05/2023	Area (km^2)	132.23	151.64	248.43	343.25	476.53	495.99	312.40	42.45
	Area (%)	6.00	6.88	11.27	15.58	21.63	22.51	14.18	1.92
27/10/2022	Area (km^2)	63.31	86.89	268.89	1064.66	719.72	0	0	0
	Area (%)	2.87	3.94	12.20	48.32	32.65	0	0	0
28/11/2022	Area (km^2)	3.49	20.00	243.38	1929.47	5.66	0	0	0
	Area (%)	0.15	0.91	11.04	87.58	0.25	0	0	0

experienced AET values ranging from 5 to 6 mm/day and an additional 42.45 km^2 area had AET rates falling between 6 to 7 mm/day. During the months of October, November and January, the rate of actual evapotranspiration (AET) consistently ranged between 2 to 3 mm/day, covering more than 60% of the study area. This pattern could be attributed to the presence of low net radiation during these months. A significant portion of the study area experiences AET rates ranging from 3 to 6 mm/day during the majority of the summer months. This pattern is observed across over 65% of the study area. It's important to remember that AET rates can be affected by various factors, including temperature, humidity, wind speed, solar radiation, vegetation cover and soil type. These variables can differ based on the geographical location, leading to variations in the observed AET rates (Feng *et al.*, 2020).

4.3. *Comparing maximum regional SEBAL Actual ET (AET) with Potential ET (PET)*

To compare and validate evapotranspiration estimates, a common approach involves combining meteorological data - driven techniques with remote sensing methods (Nouri *et al*., 2016) because the scarcity of lysimeters in the study area. Daily potential evapotranspiration was determined through the application of FAO Penman - Monteith method and various empirical method, as detailed in Table 3. The maximum AET rate obtained from the SEBAL algorithm were compared and verified against the potential evapotranspiration rates calculated using the corresponding empirical formulas (Table 3). The findings revealed a notably highly positive correlation, low RMSE in mm/day and strong agreement between the maximum AET rate and PET calculated using

TABLE 3

Comparision of maximum actual evapotranspiration (Max. AET) from SEBAL with potential ET (PET) from empirical methods

Date	Max. AET from SEBAL	Empirical method of PET measurement (mm/day)				
		FAO Penman-Monteith	Modified Penman	Hargreaves	Turc	Blaney Criddle
27/10/2022	3.73	4.36	3.55	4.62	4.67	4.70
28/11/2022	3.19	3.88	2.80	3.96	3.93	3.90
15/01/2023	3.07	3.70	2.71	2.96	3.49	3.49
16/02/2023	3.45	5.00	4.26	5.37	5.03	5.52
04/03/2023	4.77	4.61	3.98	6.04	4.58	4.98
21/04/2023	6.14	5.85	5.26	6.19	6.37	5.57
23/05/2023	7.17	5.82	5.30	4.92	6.35	4.97
Correlation		0.88	0.89	0.56	0.90	0.53
Index of Agreement (d)		0.83	0.86	0.67	0.88	0.59
RMSE (mm/day)		0.895	0.915	1.296	0.834	1.260

FAO Penman-Monteith, Turc and modified Penman methods. A close alignment between the maximum AET and PET rates was observed in 15-20% of the study area during the months of April and May, as indicated in Table 2. The comparison of AET and PET patterns reveals critical implications for water resource management. Identifying regions where AET and PET closely align is essential to prioritize water scarcity mitigation strategies. These strategies should focus on demand-side management, supply-side augmentation and water allocation optimization. Additionally, implementing effective drought preparedness and response plans and watershed management practices is crucial for sustainable water resource management.

5. Conclusions

The objective of this study was to assess the applicability of pySEBAL algorithms for estimating actual evapotranspiration (AET) in the study area. The pySEBAL algorithm demonstrated its potential for estimating AET, LST, albedo, NDVI, crop coefficient and different energy fluxes across large and heterogeneous study area. A fundamental advantage of remote sensing-based methods is their ability to map the spatial variability of AET across a wide range of scales. In most of the study area, AET rates are between 4 and 6 mm/day in the summer and between 2 and 3 mm/day in the winter. This pattern was observed over 65% of the study area. In May, AET rates closely match PET rates in about 15-20 % of the study area, which could indicate a potential water scarcity problem.

The 16-day temporal resolution of Landsat 8 satellite data limits pySEBAL model applicability to potential application in agriculture especially in irrigation scheduling, crop water requirement calculation and yield forecasting. This limitation originates from the infrequent estimation of AET rates due to lower temporal resolution of satellites, which are crucial for accurate decision-making in these agriculture practices. To address this temporal resolution challenge and get daily AET data, two potential solutions can be explored: (*i*) Increasing Remote Sensing Data Availability: Developing pySEBAL algorithms for multiple satellites images and combining data from multiple satellite images can further enhance data availability and improve the suitability of pySEBAL for agricultural applications, particularly in regions where lysimeters are scarce. (*ii*) Utilizing pySEBAL-derived Crop Coefficients: Integrating pySEBAL-derived crop coefficients (kc) obtained during Landsat image acquisition periods with daily reference evapotranspiration (RET) data from the FAO Penman-Monteith equation can generate daily AET estimates.

Acknowledgments

The lead author expresses gratitude to the Agrometeorology team at Navsari Agricultural University and Mr. Rafeeippo from Brazil for their invaluable guidance. Special thanks are extended to Mr. Nikhil Malaviya and Dr. Y. A. Garde for promptly providing the technical support.

Disclaimer: The contents and views expressed in this research paper/article are the views of the authors and do not necessarily reflect the views of the organizations they belong to.

References

Ajjur, S. B. and Al-Ghamdi, S. G., 2021, "Evapotranspiration and water availability response to climate change in the Middle East and North Africa", *Climatic Change*, **166**, 3, 1-18.

Allen, R. G., Tasumi, M. and Trezza, R., 2007, "Satellite-based energy balance for mapping evapotranspiration with internalized calibration (METRIC) Model", *J. Irrig. Drain. Eng.*, **133**, 4, 380-394.

Allen, R. G., Burnett, B., Kramber, W., Huntington, J., Kjaersgaard, J., Kilic, A. and Trezza, R., 2013, "Automated calibration of the metric-landsat evapotranspiration process", *J. Am. Water Resour. Assoc.*, **49**, 3, 563-576.

Bastiaanssen, W. G. M., 2000, "SEBAL-based sensible and latent heat fluxes in the irrigated Gediz Basin, Turkey", *J. Hydrol.*, **229**, 1, 87-100.

Bastiaanssen, W. G., Menenti, M., Feddes, R. A. and Holtslag, A. A. M., 1998, "A remote sensing surface energy balance algorithm for land (SEBAL)1. Formulation", *J. Hydrol.*, **212**, 198-212.

Bansouleh, B. F., Karimi, A. R. and Hesadi, H., 2015, "Evaluation of SEBAL and SEBS algorithms in the estimation of maize evapotranspiration", *Int. J. Plant Soil Sci.*, **6,** 6, 350-358.

Beg, A. A. F., Al-Sulttani, A. H., Ochtyra, A., Jarocińska, A. and Marcinkowska, A., 2016, "Estimation of evapotranspiration using SEBAL algorithm and landsat-8 data-A case study: tatra mountains region", *J. Geol. Res. Eng.*, **6**, 257-270.

Bhatt, R. and Khera, K. L., 2006, "Effect of tillage and mode of straw mulch application on soil erosion in the submontaneous tract of Punjab, India", *Soil Till. Res.*, **88**, 1, 107-115.

Caiserman, A., Amiraslani, F. and Dumas, D., 2021, "Assessment of the agricultural water budget in southern Iran using Sentinel-2 to Landsat-8 datasets", *J. Arid Environ.*, **188,** 104461.

Diak, G. R., Mecikalski, J. R., Anderson, M. C., Norman, J. M., Kustas, W. P., Torn, R. D. and DeWolf, R. L., 2004, "Estimating land surface energy budgets from space: Review and current efforts at the University of Wisconsin-Madison and USDA-ARS", *Bulletin of the American Meteorological Society*, **85**, 1, 65-78.

Feng, S., Liu, J., Zhang, Q., Zhang, Y., Singh, V. P., Gu, X. and Sun, P., 2020, "A global quantitation of factors affecting evapotranspiration variability", *J. Hydrol.*, **584**, 124688.

Li, Z., Li, Q., Wang, J., Feng, Y. and Shao, Q., 2020, "Impacts of projected climate change on runoff in upper reach of Heihe River basin using climate elasticity method and GCMs", *Sci. Total Environ.*, **716**, 137072.

McShane, R. R., Driscoll, K. P. and Sando, R., 2017, "A review of surface energy balance models for estimating actual evapotranspiration with remote sensing at high spatiotemporal resolution over large extents", *Scientific Investigations Report*, 2017-5087.

Mkhwanazi, M., Chávez, J. L. and Andales, A. A., 2015, "SEBAL-A: A remote sensing ET algorithm that accounts for advection with limited data. Part I: Development and validation", *Remote Sensing*, **7**, 11, 15046-15067.

Norman, J. M., Kustas, W. P. and Humes, K. S., 1995, "A two-source approach for estimating soil and vegetation energy fluxes in observations of directional radiometric surface temperature", *Agric. For. Meteorol.*, **77**, 263-293.

Nouri, H., Glenn, E. P., Beecham, S., Chavoshi Boroujeni, S., Sutton, P., Alaghmand, S. and Nagler, P., 2016, "Comparing three approaches of evapotranspiration estimation in mixed urban vegetation: Field-based, remote sensing-based and observational-based methods", *Remote Sensing*, **8**, 6, 492.

Pielke, R. A., Avissar, R., Raupach, M., Dolman, A. J., Zeng, X. and Denning, A. S., 1998, "Interactions between the atmosphere and terrestrial ecosystems: influence on weather and climate", *Global change biology*, **4**, 5, 461-475.

Rahimi-Moghaddam, S., Kambouzia, J. and Deihimfard, R., 2018, "Adaptation strategies to lessen negative impact of climate change on grain maize under hot climatic conditions: a model-based assessment", *Agric. For. Meteorol.*, **253**, 1-14.

Saboori, M., Mokhtari, A., Afrasiabian, Y., Daccache, A., Alaghmand, S. and Mousivand, Y., 2021, "Automatically selecting hot and cold pixels for satellite actual evapotranspiration estimation under different topographic and climatic conditions", *Agric. Water Manage.*, **248**, 106763.

Sawadogo, A., Hessels, T. İ. M., Gündoğdu, K. S., Demir, A. O., Mustafa, Ü. N. L. Ü. and Zwart, S. J., 2020, "Comparative analysis of the pysebal model and lysimeter for estimating actual evapotranspiration of soybean crop in Adana, Turkey", *Int. J. Eng. and Geosci.*, **5,** 2, 60-65.

Sellers, P. J., Randall, D. A., Collatz, G. J., Berry, J. A., Field, C. B., Dazlich, D. A. and Bounoua, L., 1996, "A revised land surface parameterization (SiB2) for atmospheric GCMs. Part I: Model formulation", *J. climate*, **9**, 4, 676-705.

Senay, G. B., Bohms, S., Singh, R. K., Gowda, P. H., Velpuri, N. M., Alemu, H. and Verdin, J. P., 2013, "Operational evapotranspiration mapping using remote sensing and weather datasets: a new parameterization for the SSEB approach", *J. Am. Water Resour. Assoc*., **49**, 577-591.

Silva, B. B. D., Braga, A. C., Braga, C. C., de Oliveira, L. M., Montenegro, S. M. and Barbosa Junior, B., 2016, "Procedures for calculation of the albedo with OLI-Landsat 8 images: Application to the Brazilian semi-arid", *Rev. Bras. Eng. Agríc. Ambient.*, **20**, 3-8.

Su, Z., 2002, "The Surface Energy Balance System (SEBS) for estimation of turbulent heat fluxes", *Hydrol. Earth Syst. Sci.*, **6**, 1, 85-100.

Sun, Z., Wei, B., Su, W., Shen, W., Wang, C., You, D. and Liu, Z., 2011, "Evapotranspiration estimation based on the SEBAL model in the Nansi Lake Wetland of China", *Math. Comput. Modelling*, **54**, 3, 1086-1092.

Wagle, P., Bhattarai, N., Gowda, P. H. and Kakani, V. G., 2017, "Performance of five surface energy balance models for estimating daily evapotranspiration in high biomass sorghum", *J. Photogramm. Remote Sens.*, **128**, 192-203.

Wang, W., Li, C., Xing, W. and Fu, J., 2017, "Projecting the potential evapotranspiration by coupling different formulations and input data reliabilities: The possible uncertainty source for climate change impacts on hydrological regime", *J. Hydrol.*, **555**, 298-313.

Waters, R., 2002, "Surface Energy Balance Algorithms for Land-Idaho Implementation", Waters Consulting and University of Idaho and Water Watch Inc., Nelson British Columbia.

Xue, J., Bali, K. M., Light, S., Hessels, T. and Kisekka, I., 2020, "Evaluation of remote sensing-based evapotranspiration models against surface renewal in almonds, tomatoes and maize", *Agric. Water Manage.*, **238**, 106228.

Zhang, X. C., Wu, J. W., Wu, H. Y. and Li, Y., 2011, "Simplified SEBAL method for estimating vast areal evapotranspiration with MODIS data", *Water Sci. Eng.*, **4**, 1, 24-35.